International Journal of GEOMATE, Oct., 2021, Vol.21, Issue 86, pp.48-54
ISSN: 2186-2982 (P), 2186-2990 (O), Japan, DOI: https://doi.org/10.21660/2021.86.j2270
Geotechnique, Construction Materials and Environment

LIQUEFACTION RISK ASSESSMENT IN THE 23 WARDS OF TOKYO USING ELASTOPLASTIC ANALYSIS

*Kazuya Honda[1], Tomohide Takeyama[2], Shinya Tachibana[3] and Atsushi Iizuka[3]

[1]Tokyo Electric Power Services Co., Ltd., Japan
[2]Department of Civil Engineering, Kobe University, Japan
[3]Research Center for Urban Safety and Security, Kobe University, Japan

*Corresponding Author, Received: 19 July 2021, Revised: 14 Sept. 2021, Accepted: 23 Sept. 2021

ABSTRACT: The risk assessment of liquefaction damage is crucial for recovery from large-scale earthquakes, which are predicted to occur in recent years. In this study, the liquefaction risk is evaluated over a wide area through effective stress analysis, considering the interaction between the soil particles and pore water. The target area of the analysis was the 23 wards of Tokyo, including the zero-meter zone, and a 3D ground model was constructed from the borehole data. A vertical columnar ground model is established at 463 locations from the 3D ground model using the material parameter determination flow. The liquefaction risk of a wide area is evaluated by performing seismic response analysis using two types of earthquake motions for each analysis point, thus showing the difference in the risk and degree of liquefaction by location. In the future, various dynamic analyses must be conducted with sufficient resolution and compared with the actual damages.

Keywords: Elastoplastic constitutive model, Soil-water coupled problem, Finite Element Method, Liquefaction

1. INTRODUCTION

In recent years, concerns about the occurrence of large-scale earthquakes in Japan have been increasing. It is necessary to take sufficient preventive measures against earthquakes, as they are difficult to predict and cause various types of damage, such as building destruction, tsunamis, and landslides. However, the degree of damage caused by earthquakes depends primarily on the scale of the earthquake, region of occurrence, and timing. Therefore, it is necessary to evaluate the risk of the potential damage and take appropriate measures.

This study focuses on the liquefaction damage caused by earthquakes. Liquefaction damage does not generally cause direct human casualties but results in catastrophic damage to structures. Therefore, a liquefaction risk assessment is crucial for recovery from earthquakes.

Local governments have prepared hazard maps to determine the liquefaction risk using a simple assessment method based on the liquefaction resistance factor (FL) and liquefaction potential factor (PL) [1]. The FL and PL values are evaluated based on the N-value, grain size, and surface seismic intensity of the target earthquake. Liquefaction damage has been observed in a wide range of areas after the 2011 Tohoku earthquake off the Pacific Coast. Ref.[2] compared the liquefaction risk based on the FL and PL values with the actual liquefaction damage caused by the Tohoku earthquake. They observed that there was no liquefaction damage in the areas where the risk was considered to be low based on the FL and PL values. However, liquefaction was not found at several sites, even though these sites were considered high-risk areas. An overestimation of the liquefaction risk may increase the cost of the preventive measures, reduce the reliability of the estimates, and weaken the sense of crisis.

Herein, liquefaction is assessed by calculating the increase in the excess pore water pressure due to seismic motion through an effective stress analysis process, which is based on an elastoplastic constitutive model. The liquefaction risk is estimated by considering the interaction between the soil particles and the pore water. Additionally, the flow of determining the material parameters from the N-value and plasticity index allows for the material parameters to be mechanically determined from the borehole data. The liquefaction assessment was conducted for a wide area of Tokyo using a vertical columnar ground model, which is created based on the borehole data. Borehole data is a ground survey data, which mainly includes N-value and soil classification. In this study, material parameters for sandy soil and gravel are determined based on the N-value. The parameters for clay and silt are determined based on the plasticity index.

The rest of this article is organized as follows. Section 2 describes the numerical model. Section 3 describes the analysis method. In this method, a 3D ground model of the target area is first constructed from borehole data. Next, a columnar ground model of representative analysis points is created from the 3D ground model. Finally, liquefaction analysis is

performed at each points, and the liquefaction risk of the wide area is evaluated. Section 4 describes the analysis results. Section 5 concludes this article.

2. NUMERICAL MODEL

In this study, an elastoplastic dynamic analysis is performed considering the interaction between the soil particles and pore water. The soil–water coupled elastoplastic finite element program, DACSAR-I [3], was developed and applied. This section explains the governing equations and the constitutive model used in the program.

2.1 Governing Equations

The governing equations are as follows:

$$\rho\ddot{\boldsymbol{u}} + \nabla\cdot\boldsymbol{\sigma} - \rho\boldsymbol{b} = 0\,, \tag{1}$$

$$\dot{\varepsilon}_v - \nabla\cdot\boldsymbol{w} - \frac{n}{K_w}\dot{p}_w = 0\,, \tag{2}$$

$$\boldsymbol{\sigma} = \boldsymbol{\sigma}' + p_w\boldsymbol{1}\,, \tag{3}$$

$$\dot{\boldsymbol{\sigma}}' = \boldsymbol{C}:\dot{\boldsymbol{\varepsilon}}\,, \tag{4}$$

$$\boldsymbol{\varepsilon} = -\left(\nabla\otimes\boldsymbol{u} + \boldsymbol{u}\otimes\nabla\right)/2\,, \tag{5}$$

$$\boldsymbol{w} = -\boldsymbol{k}\cdot\nabla h\,. \tag{6}$$

Eqs. (1) and (2) represent the conservation of momentum and mass, respectively. Eqs. (4)–(7) represent the principle of effective stress, constitutive equation, strain–displacement relation, and Darcy's law, where ρ is the density of soil; $\boldsymbol{u}$ is the displacement vector; $\boldsymbol{\sigma}$ is the stress tensor; $\boldsymbol{b}$ is the body force vector; $\boldsymbol{\varepsilon}_v$ is the volumetric strain; $\boldsymbol{w}$ is Darcy's velocity; n is the porosity; K_w is the bulk modulus of pore water; p_w is the pore water pressure; $\boldsymbol{\sigma}$ is the effective stress tensor; $\boldsymbol{1}$ is the second-order identity tensor; $\boldsymbol{C}$ is the constitutive tensor; $\boldsymbol{\varepsilon}$ is the strain tensor; $\boldsymbol{k}$ is the hydraulic conductivity tensor; and, h is the total water head. The compression is determined to be positive. The displacement, $\boldsymbol{u}$, and pore water pressure, p_w, can be obtained by solving the governing equations for the given boundary and initial conditions.

2.2 Constitutive Model

The constitutive model employed in the analysis is based on the EC model [4]. The yield function of the EC model is expressed as follows:

$$f = \mathrm{M}D\ln\frac{p'}{p'_0} + \frac{\mathrm{M}D}{n_E}\left(\frac{\eta^*}{\mathrm{M}}\right)^{n_E} - \varepsilon_v^p = 0 \tag{7}$$

where M is the critical state parameter, D is the coefficient of dilatancy [5], p' is the effective mean stress, p'_0 is the effective mean stress in the pre-consolidated state, ε_v^p is the plastic volumetric strain, n_E is the parameter used to fit the contractancy response of the EC model to the experimental results, and η^* is the generalized stress ratio.

The EC model is integrated with the extended subloading surface model, rotationally hardening model, and shear hardening/softening model [6, 7] to describe the cyclic behavior of the soil due to earthquakes. The extended subloading surface with the aforementioned hardening rules is given as:

$$\bar{f} = \mathrm{M}D\ln\frac{\overline{p}'}{p'_0} + \frac{\mathrm{M}D}{n_E}\left(\frac{\overline{\eta}^*}{\mathrm{M}}\right)^{n_E} - MD\ln R - H = 0 \tag{8}$$

where $\overline{\boldsymbol{\sigma}}' = \boldsymbol{\sigma}' - (1-R)\boldsymbol{\alpha}$ is the modified effective stress, where $\boldsymbol{\alpha}$ represents the similarity center of the subloading surface, R is the similarity ratio of the subloading surface corresponding to the normal yield surface, and H is the hardening parameter used to represent the shear-induced hardening/softening. $\overline{p}'$ and $\overline{\eta}^*$ are the effective mean stress and generalized stress ratio, respectively, in terms of the modified effective stress. The generalized stress ratio is expressed as follows:

$$\overline{\eta}^* = \sqrt{\frac{3}{2}}\left\|\overline{\boldsymbol{\eta}} - \boldsymbol{\eta}_e\right\| \tag{9}$$

where $\overline{\boldsymbol{\eta}} = \overline{\boldsymbol{s}}/\overline{p}'$ is the stress ratio tensor, and $\boldsymbol{\eta}_e$ is the stress ratio tensor representing the stress anisotropy. The laws for developing R, $\boldsymbol{\alpha}$, $\boldsymbol{\eta}_e$, and H are as follows:

$$\dot{R} = -\frac{m}{D}\ln R\left\|\dot{\boldsymbol{\varepsilon}}^p\right\|\,, \tag{10}$$

$$\dot{\boldsymbol{\alpha}} = c\left\|\dot{\boldsymbol{\varepsilon}}^p\right\|(\boldsymbol{\sigma}' - \boldsymbol{\alpha}) + \frac{1}{p'_c}\left\{\dot{p}'_c - \dot{\boldsymbol{\eta}}_e\frac{\partial f_\alpha}{\partial\boldsymbol{\eta}_e}\right\}\boldsymbol{\alpha}\,, \tag{11}$$

$$\dot{\boldsymbol{\eta}}_e = \frac{b_r}{D}\left\{M_r(\boldsymbol{\eta} - \boldsymbol{\eta}_e) - \|\boldsymbol{\eta} - \boldsymbol{\eta}_e\|\boldsymbol{\eta}_e\right\}\left\|\dot{\boldsymbol{\varepsilon}}_d^p\right\|\,, \tag{12}$$

$$\dot{H} = \dot{\varepsilon}_v^p + \sqrt{2/3}\mu\left\|\dot{\boldsymbol{\varepsilon}}_d^p\right\|(\eta - M_d)\,, \tag{13}$$

where m is the parameter that controls the speed of the subloading surface to approach the normal yield surface; c controls the speed of the similarity center; b_r controls the rotational speed of the yield surface; M_r defines the rotational limit of the yield surface; μ controls the contribution of the shear; and, M_d defines the boundary of the hardening and softening.

3. ANALYSIS METHOD

3.1 Target Area

In this study, a liquefaction risk assessment is

conducted for the 23 wards of Tokyo, including the zero-meter zone. The eastern part of the 23 wards of Tokyo contains a wide area, called the zero-meter zone, where the elevation is below the mean sea level at high tide. There was a large-scale ground settlement in this area due to the excessive pumping of groundwater during rapid economic growth. Pumping restrictions were implemented to recover the groundwater level when the settlement became a problem, and the settlement subsided, but the ground level is still low. Although levees and sluice gates have been constructed, the ground level is still lower than the sea level, and if the flood control function is lost due to disasters such as earthquakes, typhoons, and heavy rains, it can result in extensive damage.

3.2 Creation of Ground Model

To perform the liquefaction analysis, the 16069 borehole data provided by the Civil Engineering Support and Training Center of the Tokyo Metropolitan Government is used as the geotechnical information. Fig. 1 shows the locations of the boreholes. The analysis of a large area such as the 23 wards of Tokyo requires the interpolation of the data between each boring point. This study employs a program to construct a 3D grid model developed by [8]. program to construct a 3D grid model developed by [8]. This program can construct a 3D model in the voxel format from the borehole data in the XML format. Consequently, a

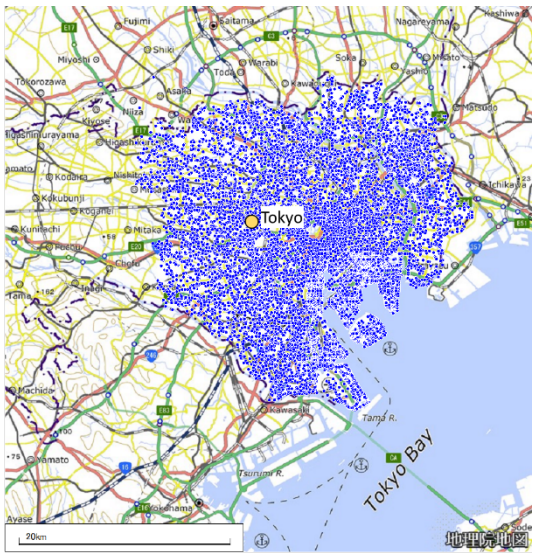

Fig. 1 Position of borehole data; the map was created by adding borehole data to GIS tiles

3D geotechnical model of N-value and soil classifications was constructed from the 16069 borehole data from the 23 wards of Tokyo using this program. The 3D ground models were constructed at intervals of 100 m along the east–west direction, 100 m along the north–south direction, and 1 m along the vertical direction. Figs. 2 and 3 show the distribution of the N-value and soil classification of the ground model for the 23 wards, respectively.

3.3 Material Parameters

The parameters required for elastoplastic analysis were determined from the N-value and soil classification data. The method proposed in [9] was used to determine the parameters based on the N-value for sandy soil and gravel. For clay and silt, the method proposed in [10] was used to determine the parameters based on the plasticity index. Figs. 4 and 5 show the flow of the material parameter determination. The results of the soil tests in the liquefaction prediction report published by the Tokyo Metropolitan Government [11] were used as a reference for each soil category, as shown in

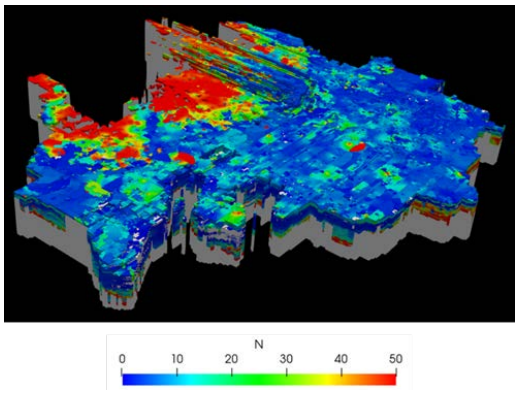

Fig. 2 3D ground model for N-value

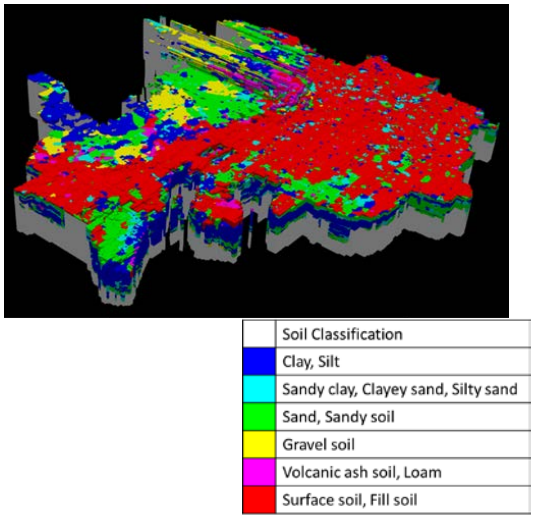

Fig. 3 3D ground model for soil classification

Tables 1 and 2. Hydraulic conductivity was specified as a general value for each soil category based on the Japanese Geotechnical Society

Standards [12]. The parameters specific to each plastic hardening model were empirically set, as listed in Table 3.

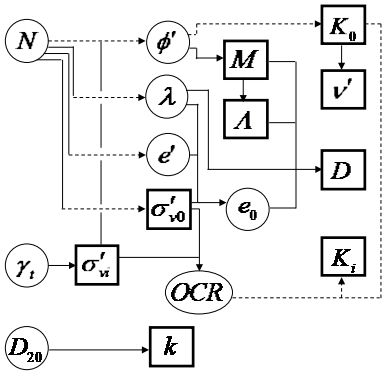

(1) $\phi' = 1.85\left(\frac{N}{(\sigma'_w/98)+0.7}\right)^{0.6} + 26$

(2) $\lambda = -0.016\ln N + 0.08$

(3) $e' = -0.15\ln N + 1.0$

(4) $\sigma'_{v0} = 40N$

(5) $M = 6\sin\phi'/(3-\sin\phi')$

(6) $\Lambda = M/1.75$

(7) $K_0 = 1-\sin\phi'$

(8) $\nu' = K_0/(1+K_0)$

(9) $OCR = \sigma'_{v0}/\sigma'_{vi}$

(10) $e_0 = e' - \lambda\ln(\sigma'_{v0}/98)$

(11) $D = \lambda\Lambda/M(1+e_0)$

(12) $K_i = K_0(OCR)^{\sin\phi'}$

(13) $k = 0.0034D_{20}^{2.2954}$

Fig. 4 Material parameter determination flow from N-value

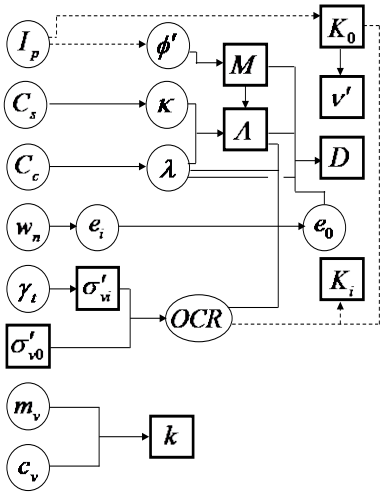

(1) $\sin\phi' = 0.81 - 0.233\log I_p$

(2) $M = 6\sin\phi'/(3-\sin\phi')$
$\Lambda = M/1.75$

(4) $K_0 = 0.44 + 0.0042I_P$

(5) $\nu' = K_0/(1+K_0)$

(6) $\kappa = 0.434C_s$

(7) $\lambda = 0.434C_c$

(8) $\Lambda = 1-\kappa/\lambda$

(9) $e_i = G_s w_n$

(10) $OCR = \sigma'_{v0}/\sigma'_{vi}$

(11) $e_0 = e_i - \lambda(1-\Lambda)\ln(OCR)$

(12) $D = \lambda\Lambda/M(1+e_0)$

(13) $K_i = K_0(OCR)^{0.54\exp(-I_P/122)}$

(14) $k = m_v c_v \gamma_w$

Fig. 5 Material parameter determination flow from plasticity index

Table 1 Applied parameters for clayey soil

Classification of soil	γ_t (kN/m^3)	I_p	k (m/s)
Clay, Mud	15.7	31	1.0×10^{-8}
Silt	17.5	15	1.0×10^{-6}
Organic soil, Peat	12.9	90	1.0×10^{-6}
Volcanic soil, Loam	13.6	54	1.0×10^{-4}

Note: γ_t is the unit weight of soil, I_p is the plasticity index, and k is the coefficient of permeability.

Table 2 Applied parameters for sandy soil

Classification of soil	γ_t (kN/m^3)	I_p	k (m/s)
Sand	19.0	-	1.0×10^{-4}
Gravel	20.1	-	1.0×10^{-2}
Backfill, Embankment, Waste	17.8	-	1.0×10^{-6}

Note: γ_t is the unit weight of soil, I_p is the plastic index, and k is the coefficient of permeability.

Table 3 Parameters for the plastic hardening models

Classification of soil	n_E	m	c	μ	M_d	b_r	M_r
Clayey soil	1.5	0.1	10	-	-	1.0	0.5
Sandy soil	1.2	0.1	30	2.0	0.8	1.0	0.5

3.4 Conditions of Analysis

Dynamic analysis was conducted at several locations in the 23 wards to assess the liquefaction risk over a wide area. The analysis points were set at intervals of 1000 m along the east–west and north–south directions in the constructed three-dimensional (3D) ground model. The distribution of the N-value and the soil classification at each analysis point were extracted, and the material parameters were determined using the method to create a columnar ground model of 463 points. Each columnar model was independently subjected to seismic analysis to evaluate the liquefaction risk at each location. For each vertical column, the top surface was assumed to be drained because of the ground surface, and the other boundary surfaces were assumed to be undrained. Both sides were set to the periodic boundary condition, and the acceleration of the target earthquake motion was applied to the bottom surface as the boundary condition. Two types of earthquake ground motions are used in this study. One is the waveform of the Tohoku earthquake off the Pacific Coast observed at the Shinagawa Seismic Observatory, which is available on the website of the Bureau of Port and Harbor, Tokyo Metropolitan Government [13]. The second is the L2 waveform of the Taisho Kanto earthquake at the Port of Tokyo, which is available on the website of the Bureau of Port and Harbor, Tokyo Metropolitan

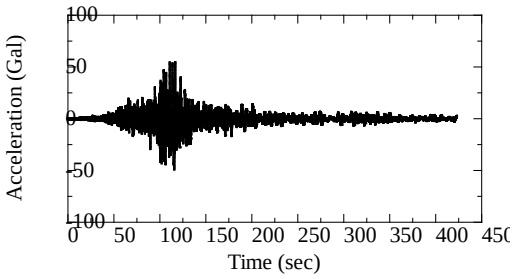

Fig. 6 Input acceleration waveform of off the Pacific Coast of Tohoku Earthquake

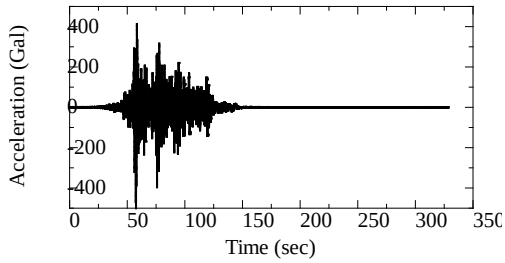

Fig. 7 Input acceleration waveform of Level 2 earthquake of the Taisho Kanko Earthquake

Government [14]. Figs. 6 and 7 present the acceleration waveforms. The difference between the two waveforms is that the maximum acceleration of the Tohoku earthquake is lower than that of the Taisho Kanto L2 earthquake; however, the acceleration is small and sustains for a long time.

4. RESULTS OF THE ANALYSIS

Figs. 8 and 9 present the maximum values of the excess pore water pressure ratio at each location, which are obtained from the analysis. However, liquefaction damage near the ground surface is unlikely despite the increase in the excess pore water pressure deep underground. Therefore, Figs. 8 and 9 show the maximum value of the excess pore water pressure ratio in the ground, which is shallower than 30 m. The excess pore water pressure ratio was calculated by dividing the excess pore water pressure by the initial vertical effective stress. It is generally assumed that liquefaction occurs when the excess pore water pressure ratio exceeds 0.95. Figs. 8 and 9 show the difference in the liquefaction risk for each location. In the case of the Taisho Kanto L2 earthquake, the increase in the excess pore water pressure ratio was more than that in the case of the Tohoku earthquake. This can be attributed to the fact that the maximum acceleration of the Taisho Kanto L2 earthquake used for input was larger than that of the Tohoku earthquake. Conversely, there were points where the excess pore water pressure ratio in the case of the Tohoku earthquake was slightly higher than that in the case of the Taisho Kanto L2 earthquake. It was assumed that the duration of the earthquake motion affected the liquefaction evaluation. In the analysis, the southern part of Koto-ku (the waterfront area) had a high liquefaction risk in both cases. Additionally, there are discrete areas with high liquefaction risk around rivers such as the Arakawa and Nakagawa. The estimation results show that high liquefaction risk in the coastal and riverine areas are alarming because embankments, sluice gates, and other tide-protection facilities are constructed in these low-lying areas to protect them from flooding. Figs. 10 and 11 show the distribution of the maximum excess pore water pressure ratio at each analysis point. Although the maximum excess pore water pressure ratio at each analysis point shown in Figs.

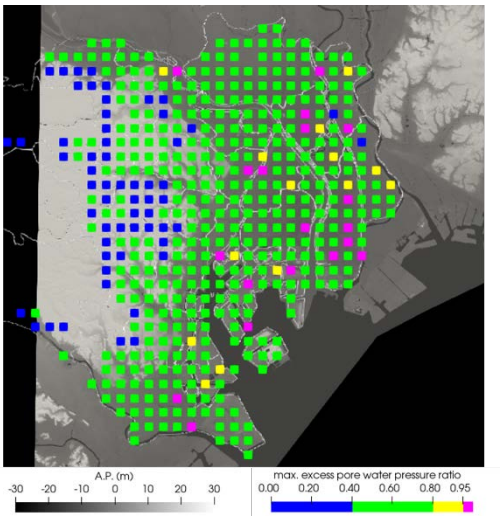

Fig. 8 Maximum excess pore water pressure ratio at each analysis point (off the Pacific Coast of Tohoku Earthquake)

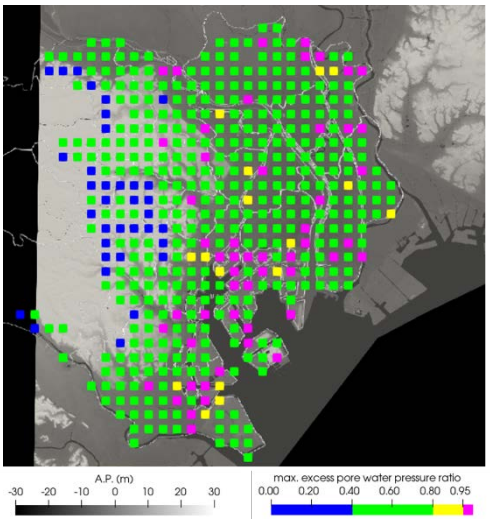

Fig 9. Maximum excess pore water pressure ratio at each analysis point (Level 2 of the Taisho Kanto Earthquake)

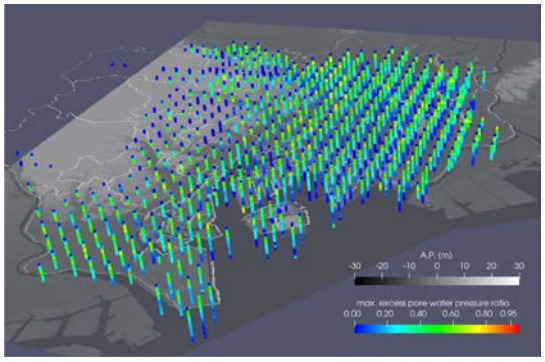

Fig. 10 Depth distribution of maximum excess pore water pressure ratio (off the Pacific Coast of Tohoku Earthquake)

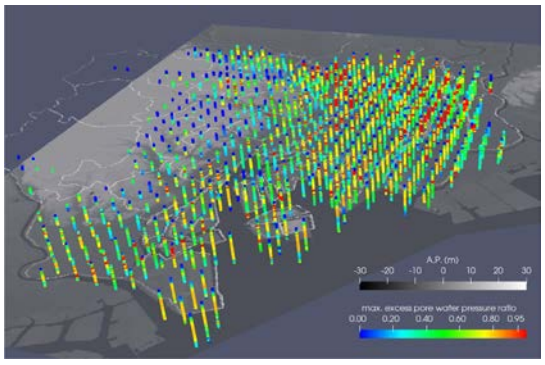

Fig. 11 Depth distribution of maximum excess pore water pressure ratio (Level 2 earthquake of the Taisho Kanto Earthquake)

8 and 9 did not show the expected difference in the degree of liquefaction, Figs. 10 and 11 show that there are more layers of high excess pore water pressure ratio in the cases of the Tohoku earthquake and Taisho Kanto L2 earthquake. Fig. 11 shows that there is a difference in the degree of liquefaction that is expected to occur in the cases of the Tohoku earthquake and the Taisho Kanto L2 earthquake.
Figs. 12 and 13 show the distribution of the maximum acceleration at the ground surface. The maximum acceleration is considered to be low because the acceleration is not sufficiently transmitted to the shallow liquefaction layer in the area where the excess pore pressure ratio increases and liquefaction occurs. However, in this analysis, the input depth is different for each point, and the same input acceleration is set for all the points. This difference in the input depth is considered to significantly affect the acceleration at the ground surface.

5. CONCLUSION

In this study, a liquefaction analysis with a columnar ground model was conducted for a wide area including the 23 wards of Tokyo by creating a

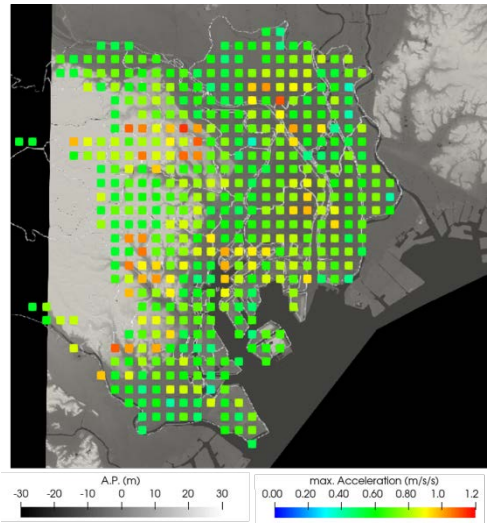

Fig. 12 Maximum surface acceleration at each analysis point (off the Pacific Coast of Tohoku Earthquake)

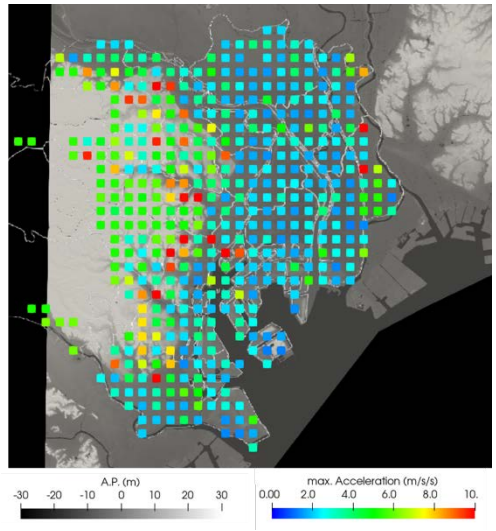

Fig. 13 Maximum surface acceleration at each analysis point (Level 2 of the Taisho Kanto Earthquake)

3D ground model from the borehole data and determining the material parameters necessary for the elastoplastic constitutive model from the ground model. Consequently, the liquefaction risk could be assessed even over a wide area using elastoplastic dynamic analysis. The liquefaction risk analysis was conducted at intervals of 1000 m. However, the resolution can be increased by decreasing the interval and assessing the liquefaction risk in greater detail.

The Tohoku earthquake and the Taisho Kanto L2 earthquake were compared, and it was observed that the Taisho Kanto L2 earthquake, which has a large maximum acceleration, has more areas with high liquefaction risk, which shows the difference

in the liquefaction risk. Conversely, there were some points where the liquefaction was assessed only in the case of the Tohoku Earthquake with a small maximum acceleration. In this study, the liquefaction risk was assessed for the Taisho Kanto L2 earthquake and the Tohoku earthquake. However, since several more earthquakes are expected to occur in the future, it is necessary to show the liquefaction risk probabilistically by analyzing various earthquake motions. The consistency must be confirmed with the actual liquefaction damage; however, in this study, the interval between the analysis points was too large to compare with the actual measurement. In the future, we will analyze with sufficient resolution and compare with the actual damage.

6. ACKNOWLEDGMENTS

We are grateful to Mr. Nakayama of the Civil Engineering Support and Training Center of the Tokyo Metropolitan Government for providing us with the borehole data. This work was supported by KAKENHI Grant-in-Aid for Scientific Research (C) #20K04682.

7. REFERENCES

[1] Iwasaki, T., Tatsuoka, F., Tokita, K., and Yasuda, S., Estimation of Degree of Soil Liquefaction during Earthquakes, The Japanese Society of Soil Mechanics and Foundation Engineering, Vol. 28, No. 4, 1980, pp.23-29 (in Japanese).

[2] Sasaki, T., Ishihara, M., Tanimoto, S., and Masuyama, H., Study on Liquefaction Determining Method based on Liquefaction occurred by the 2011 off the Pacific Coast of Tohoku Earthquake, Technical Note of PWRI 4280, 2014.

[3] Takeyama, T., Tachibana, S., and Furukawa, A., A Finite Element Method to describe the Cyclic Behavior of Saturated Soil, International Journal of Material Science and Engineering, Vol. 2, Issue 1, 2015, pp.20-25.

[4] Ohno, S., Iizuka, A., and Ohta, H., Two Categories of New Constitutive Model derived from Non-Linear Description of Soil Contractancy, Journal of Applied Mechanics, Vol. 9, 2006, pp.407-414.

[5] Shibata, T., On the Volume Changes of Normally Consolidated Clays, Annuals of Disaster Prevention Research Institute, Kyoto University, Vol. 6, 1963, pp.128-134.

[6] Hashiguchi, K., Subloading Surface Model in Unconventional Plasticity, International Journal of Soils and Structures, Vol.25, No. 8, 1989, pp.917-945.

[7] Hashiguchi, K., and Chen, Z. P., Elastoplastic Constitutive Equation of Soils with the Subloading Surface and the Rotational Hardening, International Journal for Numerical and Analytical Methods in Geomechanics, Vol. 22, No. 3, 1998, pp.197-227.

[8] Kimura, K., Hanashima, Y., Ishihara, Y. and Nishiyama, S., Three-dimensional analysis of a stratigraphic surface model by the borehole data interpolation in consideration of the formation process of buried geomorphic surfaces: a case of the basal surface model of the latest Pleistocene to Holocene incised-valley fills in the northern Tokyo lowland and the southern Nakagawa lowland, central Japan, Journal of the Geological Society of Japan, Vol. 119, No. 8, 2013, pp.537-553 (in Japanese).

[9] Miyata, T., Deformation and Stability of Sandy Soil during Excavation Work, Master's thesis of Tokyo Institute of Technology, 2001.

[10] Iizuka, A., and Ohta, H., A Determination Procedure of Input Parameter in Elasto-Viscoplastic Finite Element Analysis, Soils and Foundations, Vol. 27, No. 3, 1987, pp.71-87.

[11] Civil Engineering Support and Training Center, Tokyo Metropolitan Government, Liquefaction prediction in Tokyo, 2013 (in Japanese).

[12] Japanese Geotechnical Society, Japanese Geotechnical Society Standards Laboratory Testing Standards of Geomaterials, 2000.

[13] Tokyo Metropolitan Government Bureau of Port and Harbor, Earthquake ground motions observed at the seismic observatory of the port authority, https://www.kouwan.metro.tokyo.lg.jp/business/keiyaku/kisojoho/jishindou.html, accessed on 9 July 2021.

[14] Tokyo Metropolitan Government Bureau of Port and Harbor, L2 seismic data, https://www.kouwan.metro.tokyo.lg.jp/business/l2.html, accessed on 9 July 2021.